Nano Today 53 (2023) 102045

Contents lists available at ScienceDirect

Nano Today

journal homepage: www.elsevier.com/locate/nanotoday

Functionalized carbon nano-enabled plant ROS signal engineering for growth / defense balance

Zhijiang Guo [a,1,2], Qiong Chen [b,1,2], Taibo Liang [c], Baoyuan Zhou [d], Suhua Huang [d], Xiufeng Cao [e], Xiuli Wang [a,*], Zaisong Ding [d,*], Jiangping Tu [a,*]

[a] State Key Laboratory of Silicon Materials, School of Materials Science and Engineering, Zhejiang University, Hangzhou 310027, China
[b] School of Chemistry and Chemical Engineering, University of Jinan, Jinan 250022, China
[c] Zhengzhou Tobacco Research Institute of CNTC, Zhengzhou 450001, China
[d] Institute of Crop Sciences, Chinese Academy of Agricultural Sciences, Beijing 100081, China
[e] School of Municipal & Environmental Engineering, Shandong Jianzhu University, Jinan 250101, China

ARTICLE INFO

Keywords:
Reactive oxygen species
sp^2 carbon material
Artificial stimulus
Systemic acquired acclimation
Systemic acquired resistance

ABSTRACT

The reactive oxygen species (ROS) wave plays a crucial role as an early systemic signal in nearly all environmental response pathways. Engineering on ROS signaling may be a promising strategy to modulate plant systemic acquired acclimation and systemic acquired resistance. Recently, artificial designed materials mimicking signal transduction components have attracted attention to improve plant immunity and stress acclimation. Here, we report the bioengineering of functional carbon nanoparticles (FCN) through their regulation on ROS signaling. FCN with a C:O atom ratio of 1:2.2 were synthesized by low voltage electrolysis with graphite and carboxyl were the main oxygen-containing groups on the surface of sp^2 carbon core. The active redox properties resulting from the carboxyl–rich modification provided FCN superior ROS-triggering effects compared to other carbon nanoparticles with similar core structures but different types and quantities of surface modifications. Moreover, the ROS induced by FCN were quickly scavenged to homeostasis without causing accumulation and then leading to oxidative stress. The findings from transcriptional footprinting in *Arabidopsis*'s genes revealed a typical and quick ROS signal transduction events and also the regulation of stress responses and adaptions to biotic and abiotic stresses. In addition, the application of FCN to roots have been shown to promote the growth and development of *Arabidopsis*, rice and wheat, and also the yields particularly when suffering stresses. In summary, our findings confirmed that the ROS burst triggered by FCN modulated the balance between growth and defense through transcriptome reprogramming. It indicates that nano-enabled plant engineering for ROS can provide an economical and efficient way to promote the crops yields, especially under stress conditions.

Introduction

Sessile plants continuously regulate and adapt to dynamic environments that introduce a range of stress factors, including abiotic stressors such as variations in light intensity, extreme temperatures, high salinity, and physical damage, as well as biotic stressors caused by pathogens like bacteria, fungi, and viruses. Due to their long-term evolution, these stress response programs prompt plants to allocate their limited energy and carbon resources preferentially to defense mechanisms rather than growth [1]. While beneficial for a plant's survival, active growth inhibition is undesirable for crop productivity. Recent studies have revealed the reciprocal regulation between defense signaling and growth signaling, commonly known as growth-defense trade-offs, which enables plants to reprogram growth and stress signaling at multiple levels, thereby reducing their sensitivity to environmental stress and coordinating the distribution of energy supply between growth and defense [2,3]. In response to environmental changes, a series of endogenous signals, including reactive oxygen species (ROS), various hormones and other signal molecules, are involved in transductions, along with their complex regulatory networks, which can also lead to

* Corresponding authors.
E-mail addresses: wangxl@zju.edu.cn (X. Wang), dingzaisong@caas.cn (Z. Ding), tujp@zju.edu.cn (J. Tu).
[1] These authors contributed equally to this work.
[2] These authors co first authors.

https://doi.org/10.1016/j.nantod.2023.102045
Received 23 April 2023; Received in revised form 13 October 2023; Accepted 22 October 2023
Available online 28 October 2023

changes in the transcriptome, proteome, metabolome and physiology [4–6]. Increasing evidence suggests that moderate environmental stress can improve plant growth and that plants can overcome the inherent conflict between growth and fluctuating environmental stress through systemic acquired acclimation (SAA) and systemic acquired resistance (SAR) strategies [7,8]. Indeed, simulating low-level environmental pressure through artificial stimuli can be a highly effective strategy for disrupting the homeostasis of plant growth-defense signaling [9,10].

As key signaling molecules in plants, ROS plays an important role in the response to abiotic and biotic stresses. They help plants establish defense mechanisms and restore growth capacity by mediating stress perception, integrating environmental signals, and activating stress response pathways [4,11]. ROS wave, calcium influx, changes of membrane potentials and hydraulic pressure are major early signal events triggered by plants in response to environmental stress [12]. Despite the unclear mechanisms underlying their mode of action, routes of propagation and integration, these early signal events have been shown to participate in regulating whole-plant systemic responses [4], and can rapidly propagate cell-to-cell over long distances, sometimes spanning the entire length of the plant, through vascular bundles or apoplast in plants [12]. Among these signals, ROS wave from apoplast is considered an essential signal event that alerts plants to impendent stresses and changes their 'normal' growth state to a 'stress' state [11–13]. The production of ROS waves in plants is primarily attributed to the activity of plasma membrane-localized NADPH oxidases (NOX), also known as respiratory burst oxidase homologs (RBOHs) [14]. When plants encounter stimuli, ROS are accumulated at the apoplast, which can be sensed by neighboring cells. This leads to the triggering of ROS production in adjacent cells, resulting in a self-perpetuating cascade of amplified ROS production that can propagate holistically throughout the plant [15]. ROS waves can also be triggered by almost all kinds of abiotic and biotic stresses [4,16]. As a result, artificially generating ROS waves through stimuli and disrupting ROS balance presents a promising approach for promoting plant resistance, growth, and adaptability to their environment, through a process commonly referred to as the induction of SAA and SAR within the plant [17,18].

Studies have demonstrated that engineered nanomaterials can induce an oxidative stress response in organisms, but they also hold promise as antioxidants for therapeutic applications in the treatment of various diseases [19]. Through precise engineering of the element composition, shape and size of the core of nanoparticles and the modification of their surface ligand, nanomedicines can induce or scavenge ROS in cells, thereby regulating the pathways related to oxidative stress and apoptosis [20]. While the exact structure-function relationship remains unclear, it is apparent that structural alterations in nanoparticles may influence their interactions within organisms, which include hydrophobic interactions, electrostatic interactions, hydrogen bonds, molecular recognition and chemical redox reactions [21]. Referring to the application in the medical field, it could be possible to create a new technological revolution in agricultural production with designed nanoparticles to disturb the ROS balance of plant cells, thereby coordinating plant growth and resistance [22]. In the field of plant applications, carbon nanoparticles present prospects for the next generation sustainable agriculture. Such as carbon nanotubes (CNTs) were used to promote seed germination, graphene oxide (GO) for fertilizers application and crop production, and carbon dots for root and shoot growth promotion. [23]. However, the toxic effects of carbon nanoparticles on plants should also be considered [24]. The diverse effects observed are contingent on various factors, including plant species, growth media composition, type and concentration of carbon nanoparticles, as well as the prevailing growth conditions [25]. Emerging research revealed that carbon dots sourced from biomass exhibit a remarkable ability to eliminate ROS and enhance the tolerance of sweet potatoes to salt and nutrient stress. Their functions mainly originate from the modification on the surface of the sp^2 structure by hydroxyl and carboxylation, which can directly quench ROS with cells [26]. Glucose-modified carbon dots can significantly improve the photosynthesis and yield of wheat [27], also by reducing reactive oxygen species generation. However, nanoparticles induced ROS as signals to regulate plant resistance and adaptability has not been reported.

In order to endow carbon nanoparticles with ROS triggering ability at very low dosage, in this work, we develop a carboxyl–rich functionalized carbon nanoparticles (FCN). FCN were served as low-level environmental pressure stimulus, it triggered ROS burst and induced SAA and SAR, ultimately regulated growth and defense balance. Its application in crop production may provide an economical, efficient and simple technical way to enhance crop adaptability to their environments and increase their tolerance to global climate fluctuations, thereby leading to more resilient crops with higher yields and benefiting both farmers and the global food supply.

Results and discussion

FCN is a functional nanoparticle modified by carboxylic enrichment on the surface of the sp2 carbon core

Using graphite as raw material, we conducted carboxylic modification on the sp^2 surface by electrolysis, which is an effective method to obtain carboxyl functionalized carbon nanoparticles. As shown in Fig. S1, FCN is a light brown collosol and was synthesized by a mild electrochemical method compared to the previously reported methods [28]. The transmission electron microscope (TEM) observation shows that FCN are sphere-like particles with a diameter of 2–7 nm (Fig. 1a, b), and the spacing of the crystalline lattice is about 0.36 nm (Fig. 1a), indicating the formation of graphene-like structures, also known as sp^2 structure [29]. Fourier-transform infrared (FTIR) spectroscopy of FCN (Fig. 1c) exhibits several absorption bands corresponding to the different functional groups [30], including carboxyl, ester, hydroxyl, carbonyl and ether (Table S1). The wide absorption band of FCN, at about 3000 cm^{-1}, may come from the polymerization of –COOH, which strengthens the hydrogen bond force and disperses the stretching vibration band of –OH in –COOH [31,32]. The sharp absorption band of 3600 cm^{-1} is attributed to the vibration of a phenolic hydroxyl group. The peak at 1701 cm^{-1} can be ascribed to the C═O stretching of carboxyl, ester and carbonyl. The absorption band at 1243 cm^{-1} is attributed to the C-O stretching of hydroxyl, carboxyl and ester. These oxygen-containing functional groups are more diverse than other carbon nanoparticles with typical sp^2 structures such as CNTs (Fig. S2a) and GO (Fig. S2d). The main oxygen-containing functional groups on GO are carboxyl (1728 cm^{-1}), hydroxyl (3000 cm^{-1}, 1350 cm^{-1}) and ether (1223 cm^{-1}). CNTs contain fewer types of functional groups, comprising mainly hydroxyl (3000 cm^{-1}) and ether (1067 cm^{-1}). In addition, the proportion of oxygen-containing groups is also greater in FCN. X-ray photoelectron spectroscopy (XPS) survey (Fig. 1d) shows that FCN has a C: O ratio of 1: 2.2, exhibiting an extremely higher oxygen ratio than CNTs (1: 0.04, Fig. S2b) and GO (1: 0.07, Fig. S2e). It is also much higher than that reported in carbon dots [26]. The high-resolution XPS spectra in Fig. 1e-f show the detailed information about the carbon and oxygen bonds in FCN. By calculating the peak area, the relative content of the main groups C═C: C═O: COO: C–O was found to be 1.00: 0.60: 1.00: 0.65. Comparatively, the relative content of C═C: COO: C–O in GO was observed to be 1.00: 0.15: 1.92 (Fig. S2f). CNTs contain fewer types of functional groups, with a C═C: C–O ratio of 1.00: 0.61 (Fig. S2c). These data prove that the surface of the as-prepared FCN is functionalized with an extremely rich carboxyl group (–COOH), which is also much higher than other reported carbon dots [26].

Since the thermal stability of the carboxyl group on the surface of the sp^2 structure is lower than that of other groups, such as hydroxyl, we pyrolyzed FCN at 500 °C to obtain F500, which is used as a reference material to study the effect of carboxyl group on the surface of sp^2 structure. The FCN derivative has the same crystalline lattice of about 0.36 nm (Fig. S3), indicating that the core structure is not changed by

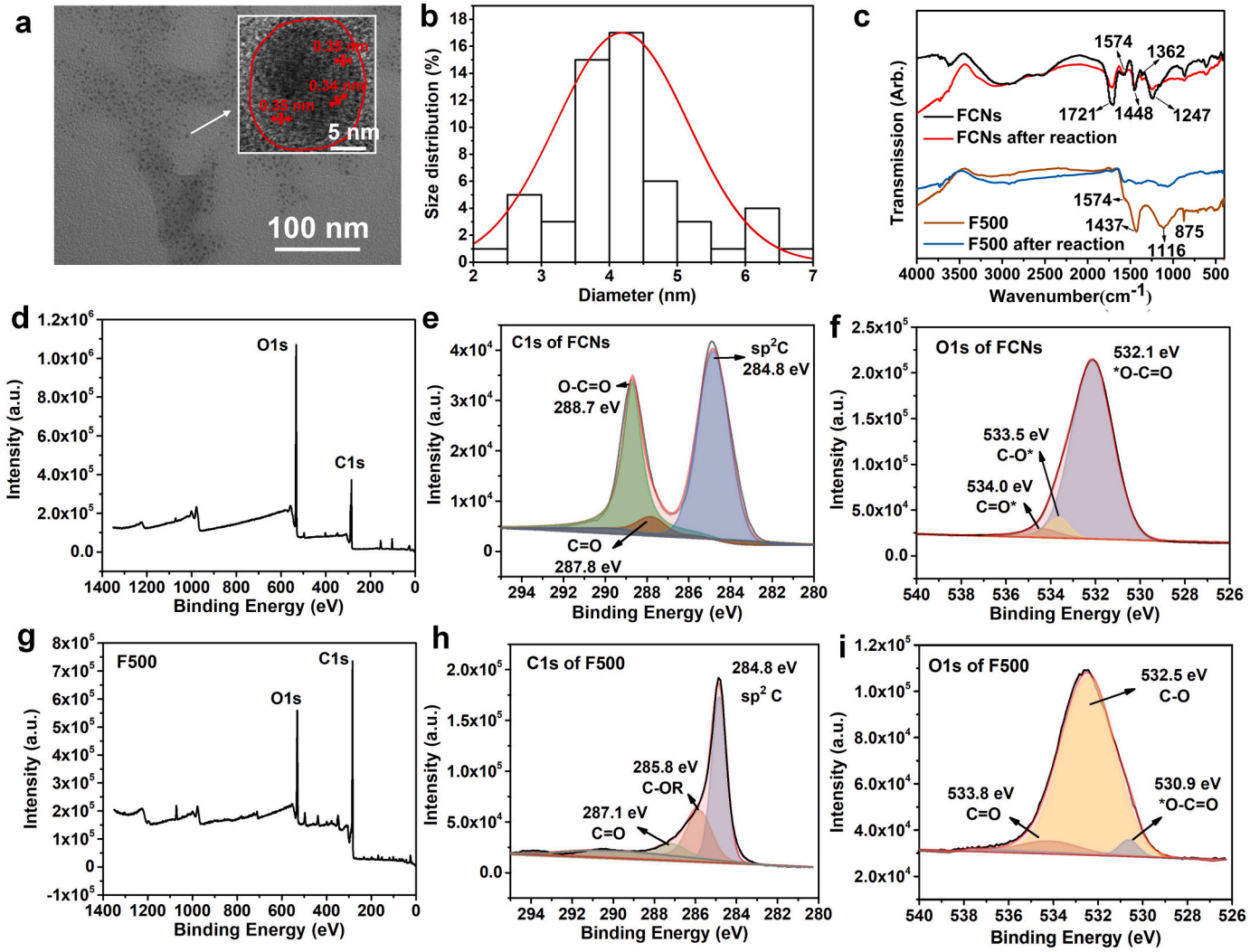

Fig. 1. FCN is characterized by high oxygen and functionalized by rich carboxyl groups. (a) TEM and HRTEM image of FCN. (b) Size distribution calculated randomly from figure (a). (c) FTIR spectra of FCN and F500 before and after reaction with H_2O_2. (d-f) XPS full scan spectrum, high-resolution XPS spectra of C 1 s and O 1 s of FCN. (g-i) XPS full scan spectrum, high-resolution XPS spectra of C 1 s and O 1 s of F500.

pyrolysis, while the ratio of C: O atom in F500 decreases to 1: 0.79 after pyrolysis (Fig. 1g). The FTIR spectrum in Fig. 1c shows that the functional groups on F500 are C═O (1569 cm^{-1}), C═C (1437 cm^{-1}), ether (C–O, 1116 cm^{-1}), and alkyl (875 cm^{-1}), and the relative content of C═C: C–O: C═O is 1: 0.47: 0.14 (Fig. 1h, i). The FTIR and XPS results indicate that C–O is the main oxygen-containing functional group in F500.

High carboxyl ligands proportion contributes to the high redox activity in FCN

The carboxyl group modification on the surface of the sp^2 structure provides carbon nanoparticles with superoxide dismutase (SOD) -like or peroxidase (POD) -like activities [33]. They are often used as antioxidants to inhibit the accumulation of ROS in cells or cell damage caused by H_2O_2 [34]. Although the catalytic activity of FCN is lower than that of biological SOD, FCN has a higher SOD-like activity under acidic conditions, which can inhibit the photochemical reduction of nitrotetrazolium blue chloride (NBT) (Fig. 2a-c). FCN also shows very high POD-like activity (Fig. 2d-f). Similar to horseradish peroxidase (HRP) from biological sources, the catalytic activity of FCN has a strong pH dependency, with an optimal pH value of 3.5 and 4.5, respectively. Their catalytic activities decrease significantly above or below the optimal pH value (Fig. 2d). At the optimal pH condition, the POD-like catalytic activity of FCN exhibits typical enzyme kinetic characteristics in response to the concentration of H_2O_2 and TMB (3,3′,5,5′ - tetramethylbenzene) substrate (Fig. S4). Its affinity for TMB substrate is higher than that of HRP, while its affinity for H_2O_2 is much lower than that of HRP. After removing –COOH by pyrolysis, the SOD- and POD-like activity of F500 show a sharp decrease (Fig. 2a-f). GO and CNT have similar structures to FCN but have lower proportions of –COOH ligands. Despite this difference, the SOD- and POD-like activities of GO and CNT are comparable to those of F500 (Fig. 2c, f). These results indicate that the modification on the surface of the sp^2 structure with rich –COOH ligands is crucial for the antioxidant activity of carbon nanoparticles.

Prior studies on the POD-like catalytic mechanism of carbon nanoparticles indicated that the O═C group might be the active site responsible for the catalytic activity, while the O═C–O– group might serve as the binding site for H_2O_2 [35]. FCN has rich O═C and O═C–O– groups, while F500, GO or CNT only has one kind of group, with low or zero content of carboxyl, O═C–O– and other surface modifications (Fig. 1i and Fig. S2c,f), which might be the structural basis for the FCN's high POD-like activity. When FCN was mixed with H_2O_2, the FTIR spectrum showed that the absorption peaks at 1701 cm^{-1} and 1243 cm^{-1} related to carboxyl and carbonyl groups decreased (Fig. 1c), indicating its reaction with H_2O_2. However, after the addition of H_2O_2,

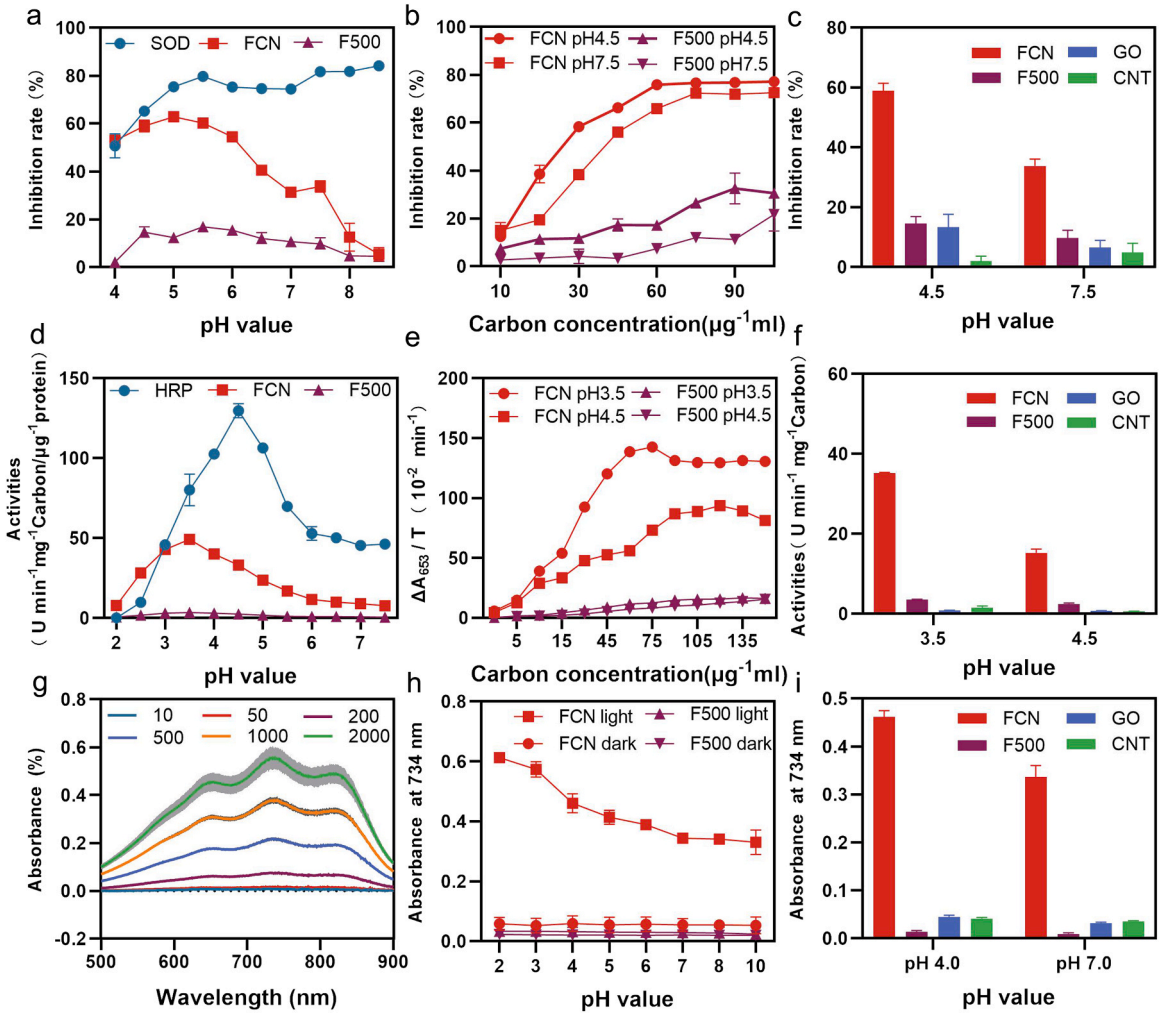

Fig. 2. SOD-, POD-like and light-catalyzed oxidase-like activities of FCN depended on functionalized carboxyl groups. (a and d) Effects of reaction pH on SOD-like and POD-like activities of FCN and F500, respectively. (b and e) Comparison of SOD-like and POD-like activities of FCN and F500 at various carbon concentrations, respectively. (c and f) SOD-like and POD-like activity of FCN and other carbon nanoparticles lacking functionalized carboxyl groups, respectively. (g) Effects of photosynthetically active radiation (PAR) on the light-catalyzed oxidase-like activity of FCN. (h) Effects of reaction pH and light on the oxidase-like activity of FCN and F500. (i) Light-catalyzed oxidase-like activity of FCN and other carbon nanoparticles lacking functionalized carboxyl groups.

the FTIR spectra of GO or CNTs did not change (Fig. S2a, d), indicating that GO and CNT did not react with H_2O_2. Although the FTIR spectrum of F500 was found to decrease in the whole band from 800 cm^{-1} to 1700 cm^{-1}, its mechanism needs further clarification.

FCN also has light-dependent oxidase activities (Fig. 2g-i). The reversible transformation between ABTS (2,2 '- Azinobis - (3-Ethyl-benzothiazoline-6-Sulfonic acid)) and its free radical state ($ABTS^+$) occurs with the redox level of the environment, which is often used to detect the level of antioxidant substances [36]. Under light conditions, FCN can oxidize ABTS into $ABTS^+$ to increase absorbance at 734 nm. The oxidization velocity was found to correlate with light density (Fig. 2g), while no oxidase activity occurred in dark conditions (Fig. 2h). Similar to the SOD- and POD-like activities, the light oxidase activity of FCN also prefers low pH conditions (Fig. 2h). However, the light-dependent oxidase activity of GO, CNT and F500 could not be detected (Fig. 2h, i), indicating that the light oxidase activity of FCN could also be related to the functionalized rich carboxyl group.

FCN has both oxidase and antioxidant enzyme-like activities, which are crucial to the regulation of ROS homeostasis in cells. The enzyme-like activities of FCN depend on its concentration during the reaction (Fig. 2b, e, and Fig. S5). The SOD- and POD-like activities peaked when the FCN concentration increased to 60 μg/mL (Fig. 2b, e). However, the rate of light oxidase-like activity was still increasing even when the concentration of FCN increased to 300 μg/mL (Fig. S5). The dose dependence of FCN's enzyme-like activities indicates that using it as an antioxidant to alleviate stress effects on plants may require a high dosage application like the reported carbon dots [26], which could also bring certain biosafety risks.

Surface carboxyl modification plays a key role in ROS bursts in plants triggered by FCN

To validate the disturbing effects of FCN on plant ROS homeostasis, ROS bursts were detected via the 2′, 7′-dichlorofluorescein diacetate (H_2DCF-DA) fluorescence image method and Luminol chemiluminescence method [37] in *Arabidopsis* leaf. Both experiments demonstrated that FCN (1.5 μg/mL) triggered a rapid process of ROS burst in apoplasts, which lasted for approximately 45 min, with the highest burst value observed between 20 and 30 min following treatment (Fig. 3a-d). In the roots, FCN treatment also induced the same pattern of ROS burst (Fig. S6). The ROS wave triggered by FCN was similar to that of plant immune elicitors (peaked in 10–20 min and eliminated in 30 min), such as Flagellin peptide (flg22) [37], N-terminus of the bacterial Elongation Factor Tu protein (elf18) [38], lipopolysaccharide [39], chitins [40], *etc*. It suggested that FCN might also be recognized by receptor-like kinases/proteins (RLKs/RLPs) in the plasma

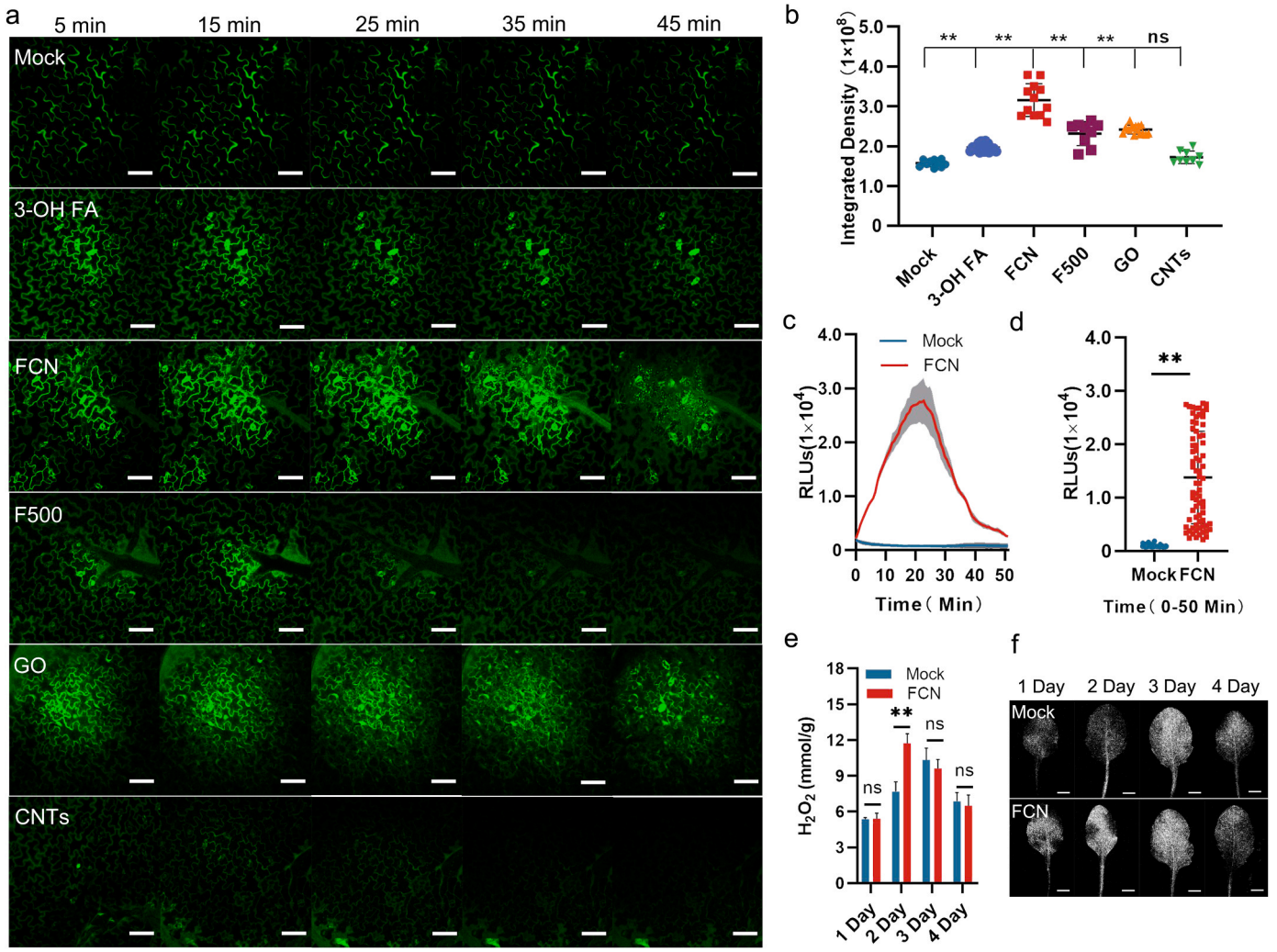

Fig. 3. FCN-triggered ROS burst is related to functionalized rich carboxyl on the surface of the sp^2 core. (a) Representative images showing ROS dynamics during 45 mins of 3-hydroxy decanoic acid, FCN, F500, GO and CNTs application on *Arabidopsis* leaves. Scale bars, 50 μm. (b) Relative DCF fluorescence intensity in (a) (n = 9 −17). (c) ROS burst detected by the luminol-horseradish peroxidase chemiluminescence method in *Arabidopsis* leaves. (d) Total photon counts calculated from (c) (n = 74). (e) H_2O_2 content after FCN spraying on leaves. (f) Representative image of the leaves stained with DAB after FCN spraying. Scale bars, 2 mm. The error bars in the columns represent the SEM, the columns labeled with "* *" indicate significant differences at $P < 0.01$, and "ns" suggests no significant difference.

membrane as which of immune elicitors, thus regulating the phosphorylation of RBOHs, activating its oxidase activity, and forming ROS burst in apoplasts [4,14]. Medium-chain 3-hydroxy fatty acid (3-OH FA), a new type of authenticated plant immune elicitors, is recognized by receptor-like kinase Lipooligosaccharide-Specific Reduced Elicitation (LORE) [41]. The medium-length carbon chain, terminal carboxyl group and free-hydroxyl group at the β position are crucial for the immune recognition of LORE. The carboxyl and hydroxyl functional groups modified on the surface of the sp^2 carbon core of FCN may also form this specific structure. It was found that the ROS wave induced by FCN was stronger and lasted longer than that by 3-hydroxydecanoic acid, the strongest in 3-OH FAs immune elicitor (Fig. 3a, b). Previous reports have shown that the magnitude of immune elicitors triggered ROS and downstream defense responses varies, depending on the concentration and respective immune elicitor [42,43], also the genes involved in RBOHD regulation [44]. Although the kinetics have not been reported yet, abiotic stress can also induce ROS burst [4]. FCN could induced both biotic and abiotic stress responses (Fig. 4, supplemental table 7). It indicated that FCN may simultaneously activate multiple signal transduction pathways to participate in the RBOHD regulation process, which resulting a stronger and longer ROS burst. In addition, a comparative analysis of the ROS burst induced by F500, GO and CNT in *Arabidopsis* leaves revealed that neither F500 nor CNT could induce ROS burst (Fig. 3a). Meanwhile, GO triggered a process of ROS burst consistent with that of FCN, albeit with a lower intensity (Fig. 3a, b), similar to the results of inducing ROS burst in the roots of *Arabidopsis* and rice (Fig. S7). From the perspective of structure, both FCN and GO have carboxyl group modification, indicating that the carboxyl group may play a major role in inducing ROS burst and increasing the amount of carboxyl group modification could improve the intensity of the induced ROS burst.

Previous study [26] found that carbon dots, modified with carboxyl and hydroxyl groups, can quench ROS at a concentration as high as 1.5 mg/mL, much higher than the treatment concentration of FCN in this study (1.5 μg/mL). Our results showed that a high concentration of FCN (15 μg/mL) treatment also led to diminished ROS levels when the root tips of *Arabidopsis* and rice were treated with 10 fold gradient increasing concentration (Fig. S8). Conversely, lower concentrations of FCN (0.15 and 1.5 μg/mL) led to an accumulation of ROS (Fig. S8). These differences could be attributed to the strong antioxidant enzyme-like activity of FCN at higher concentrations (Fig. 2b,e) that can quickly quench the ROS induced by itself [26].

Although FCN has shown promise in regulating oxidative stress in plants, it is unclear whether the ROS burst induced by FCN may interfere

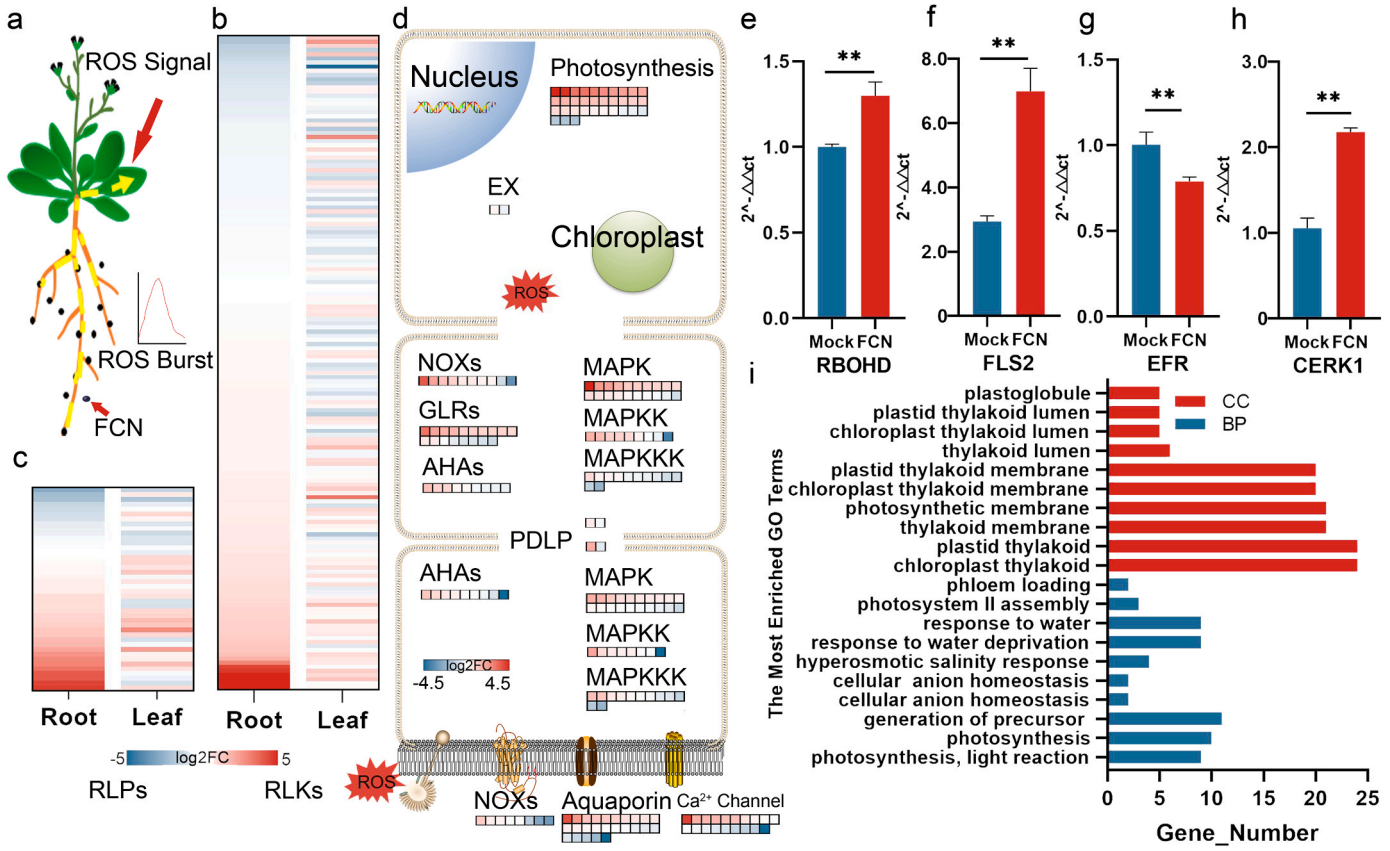

Fig. 4. FCN application on roots induces typical ROS signal transduction events in the whole plant. (a) Schematic of FCN trigger ROS and its signal transduction. (b and c) Gene expression of RLKs and RLPs in roots and leaves. (d) Gene expression in typical ROS signaling transduction. (e-h) Relative expression level of RBOHD, FLS2, ERF and CERK1. (i) Co-enrichment of GO terms in roots and leaves. CC, cell component. BP, biological process. The error bars in the columns represent the SEM. Columns labeled with "* *" indicate significant differences at $P < 0.01$.

with the cellular ROS defense system, potentially leading to ROS accumulation and further oxidative stress in living organs. Therefore, further research is needed to investigate the potential effects of ROS accumulation induced by FCN on the cellular ROS defense system and overall plant health. FCN was sprayed on *Arabidopsis* shoots, and H_2O_2 concentrations were detected in the following 4 days. The leaf H_2O_2 accumulation (Fig. 3e,f) follows a dynamic process from disturbance to equilibrium, similar to the transient ROS wave. It indicated that the environmental pressure simulated by FCN application does not exceed the regulatory capacity of the ROS-eliminating system and will not produce continuous ROS accumulation that could lead to oxidative stresses. It may also be related to the fact that FCN has SOD- and POD-like activities, which can effectively remove reactive oxygen species.

FCN induces typical ROS signal transduction events

ROS wave in response to biotic and abiotic stimuli has been linked to local and systemic signal transduction [45]. During pattern-triggered immunity, plants use pattern recognition receptors to activate NOX and yield ROS in apoplasts [46,47], then ROS passes through the aquaporin of the plasma membrane in the form of H_2O_2 [48], causing a second ROS burst in chloroplasts and regulating gene expression in the nucleus through chloroplast retrograde signaling [4,49–51]. The involvement of this signal transduction process has been confirmed in seven indicative events [52]. RNA-Seq analysis reveals that these typical signal transduction events occur in the leaves of *Arabidopsis* after 6 h of FCN treatment in rhizospheres (Fig. 4a). The related gene expressions were regulated, including RLKs and RLPs, which can recognize external stimulus [45], RBOHs that participate in ROS production [14], aquaporin PIP1;4/PIP2.1 that allow apoplastic ROS entering into the cytosol [48], ROS-dependent calcium channel GLR3.3/GLR3.6 that control extracellular and vacuole Ca^{2+} entering into cytoplasm [53], mitogen-activated protein kinase (MAPK) module coupled with Ca^{2+} [50], H^+-ATPase that coordinate ROS accumulation in apoplasts [54], PDLP5/PDLP8 regulating callose deposition on plasmodesmata [55] and ROS signal transduction in symplast [56], and EX1/EX2 that modulate chloroplast singlet oxygen [57], to affect nuclear gene expression (Fig. 4b-d, Table S2, Table S3). The gene expressions of RBOHD (Fig. 4e) and several known RLKs such as FLS2 (Fig. 4f), EFR (Fig. 4g) and CEPR1 (Fig. 4h) were assessed by qPCR, which confirmed the reliability of the RNA-Seq results. GO analysis was conducted on 142 common differentially expressed genes (DEGs) (Table S4, FDR<0.05) in roots and leaves after 6 h of FCN treatment on the plants' roots. Our analysis revealed that the DEGs in response to FCN treatment were primarily enriched in those related to chloroplast and plastid membranes regarding cellular components. In contrast, genes participating in stress response and photosynthesis were predominantly enriched in the biological processes category (Fig. 4i). These findings suggest that the ROS wave induced by FCN can rapidly regulate the expression of genes related to its signal pathway.

Laser confocal microscopy confirmed several key physiological processes involved in the transduction of ROS signals induced by FCN. In particular, we observed the binding of FCN to the plasma membrane, which suggests that it may be recognized by RLKs or RLPs (Fig. S9). In addition, we observed the influx of Ca^{2+} (Fig. S10), which is known to play a role in plant stress responses. Lastly, we observed the second production of ROS in chloroplasts (Fig. S11), further supporting the involvement of ROS in the transduction of stress signals in plants. These

results suggest that the generation of ROS wave triggered by FCN and its downstream regulation may have a similar mechanism to the plant immune recognition.

FCN induces the up-regulation of genes involved in biotic and abiotic responses

Previous studies have demonstrated that exposure to high light and high temperatures can trigger ROS waves, activating plant SAA and increasing environmental tolerance [45,58]. To study the response of plants to FCN, we sampled shoots from short (2 and 6 h) and long (15 and 30 days) time rhizosphere FCN treatment in *Arabidopsis* (Fig. 5a). A total of 528, 6029, 479, and 386 DEGs were identified with significant regulation (FDR<0.05, |log2FC=>1) across the four sampling times. These results indicate a dynamic trend observed from rapid increase to gradual stability, and little overlap of DEGs was detected among them (Fig. 5b-c, Table S5). In the short-term FCN treatment, a similar proportion of up-regulated and down-regulated DEGs was observed, whereas mainly up-regulated DEGs with few down-regulated DEGs were identified in the long-term treatment (Fig. 5b). Furthermore, the proportion of transcription factors among the DEGs increased from less than 10–50% or higher after long-term treatment (Fig. 5b). These upregulated transcription factors primarily belong to families such as WRKY, MYB, NAC, HSF, bZip, bHLH and AP2/ERF (Table S6) which play crucial roles in regulating stress and immune response [59–61]. GO annotation enrichment analysis on the 4 sampling times indicated 165–266 potential terms, in which biological process (BP) was found to contribute the most, especially in the long-term treatment (Fig. 5d, Table S7). Interestingly, we observed that the overlaps of the enriched GO terms based on the total significantly regulated DEGs were much higher than those of the DEGs (Fig. 5e, c). The 20 GO terms that were co-enriched at all four stages belong to biological processes involved in responses to various internal and external stimuli (pathogens, environmental stress, plant hormones ABA and JA etc.), and the enrichment fold increased gradually (Fig. 5f), confirming that FCN can continuously trigger the stress response of plants. Furthermore, an increasing number of genes involved in regulatory functions, such as regulation of defense response (GO:0031347), regulation of immune system process (GO:0002682), regulation of plant-type hypersensitive response (GO:0010363), regulation of response to biotic stimulus (GO:0002831), regulation of stress response (GO:0080134), regulation of signal transduction (GO:0009966), regulation of salicylic acid-mediated signaling pathway

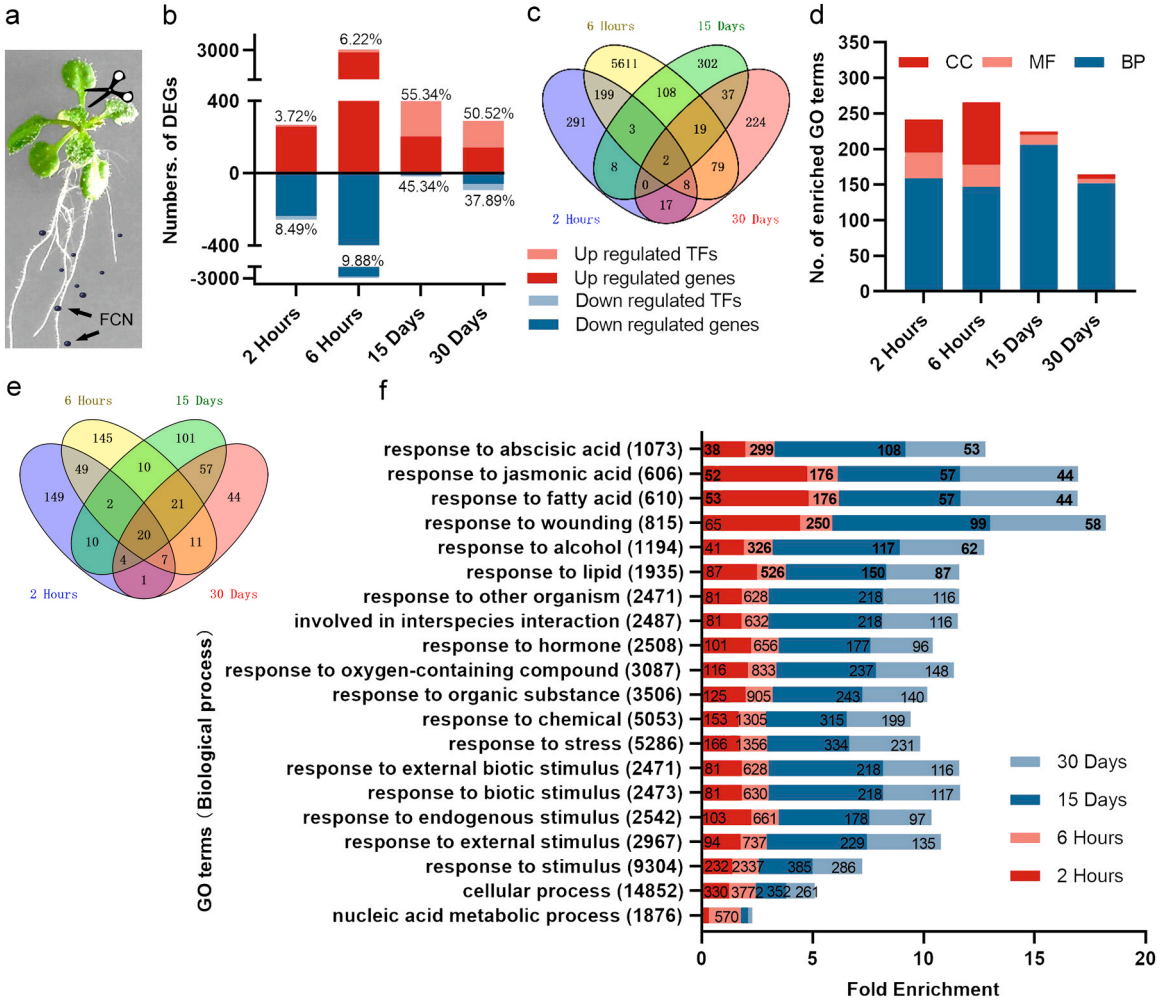

Fig. 5. FCN-induced fast responses to stimulus and stress acclimation. (a) Schematic representation of the experiments conducted. *Arabidopsis* seedlings were cultivated on solid MS medium containing FCN, and leaves were sampled after 2 h, 6 h, 15 days, and 30 days for transcriptome analysis. (b) Differential expressed genes and transcription factors in *Arabidopsis* leaves during FCN application on roots. The numerals on the bars indicate the proportions of TFs in the DEGs. (c) Venn diagrams for the overlap of the DEGs between the different FCN treatment durations. (d) Enriched GO terms between the different FCN treatment durations. CC, MF and BP indicate cellular components, molecular functions, and biological processes. (e) Venn diagrams for the overlap of the enriched GO terms between the different FCN treating durations. (f) Co-enriched GO terms between the different FCN treating durations. The numerals in the bars represent the numbers of DEGs in the GO term.

(GO:2000031), and regulation of jasmonic acid mediated signaling pathway (GO:2000022), were enriched in the long-term FCN treatment (Table S7). These findings indicate that the plant underwent a change process from a rapid response to stimulus and defense response to regulation of these responses. In addition, FCN can induce SAA and SAR in plants and may subsequently modulate the growth-defense trade-off, leading to a rapid defense response.

FCN application promotes plant growth and acclimation

FCN has been demonstrated to simulate environmental stress by disrupting ROS homeostasis and regulating the expression of SAA and SAR-related genes. Consequently, FCN may coordinate both plant defense and growth processes, promoting the growth and development of plants, particularly under conditions of environmental stress. To test this hypothesis, two model plants, *Arabidopsis* and rice, were used in the study. *Arabidopsis* growth was noticeably promoted after 15 days of growth, both in MS medium containing 1.5 μg/mL FCN and in soil with watering of 1/4 MS nutrient solution containing 1.5 μg/mL FCN (Fig. 6a, c). FCN application significantly increased biomass and seed yield (Fig. 6b,d and Fig. S13) while also promoting the absorption of various mineral nutrients (Fig. S14). These growth advantages are likely related to the strong root system (Fig. 6a). FCN triggered ROS may participated in this regulation, since ROS has been identified as a messenger in controlling plant root hair and lateral root development [62,63]. Similarly, in a three-year experiment, we found that FCN application after transplanting rice increased biomass and nitrogen accumulation in natural conditions (Fig. 6e and Fig. S14c,d), and the yields were improved dramatically by 12.0%– 19.1% (Fig. 6f-i). When *Arabidopsis* plants were cultivated under high-temperature conditions (28 °C) and watered with FCN at a concentration of 1.5 mg/L, they exhibited higher tolerance levels. Specifically, biomass and seed yield increased by 44.2% and 51.6%, respectively (Fig. S15). FCN application in rice cultivated in saline-alkali soil (pH 8.55, salt 0.26%) also resulted in a doubled grain yield (Fig. S16). Both results indicate that the effect of FCN application on yield increase was more significant under stress conditions. It suggests that FCN promotes plant acclimation to various stresses. Additionally, FCN was used as a seed-coating agent for wheat growth regulation in field conditions, resulting in a yield increase of 9.66% (Fig. S17). Recently, there has been increasing evidence showing that nanoparticles could increase stress tolerance by interfering with ROS generation [64] or elimination [26]. Our results showed that the effective concentration of FCN (1.5 mg/L) was much lower than in other studies (40 mg/L and 1.5 g/L) [26,64], while higher concentration could inhibit *Arabidopsis* growth (Fig. S18). From a biosafety standpoint, FCN exhibits significant regulatory effects on both plant growth and resistance, despite their much lower dosage requirements. These promising findings make FCN a strong candidate for agricultural applications.

Conclusion

In conclusion, our investigation suggests that carbon-based nanoparticles with sp^2 structure and carboxyl–rich modification can serve as external stimuli to mimic environmental stress, inducing plants to produce ROS signal waves and acquire systemic resistance and acclimation. The application of these nanoparticles to *Arabidopsis* and rice led to notable improvements in growth, yield, and stress tolerance, including heat and salt-alkali stress. Moreover, the SAR and SAA induced by these nanoparticles may confer tolerance to a range of pathogens and abiotic stresses. Although FCN is speculated to trigger ROS waves through a similar mechanism to immune receptor recognition, further research is required to confirm the receptor-like kinase/protein that can recognize

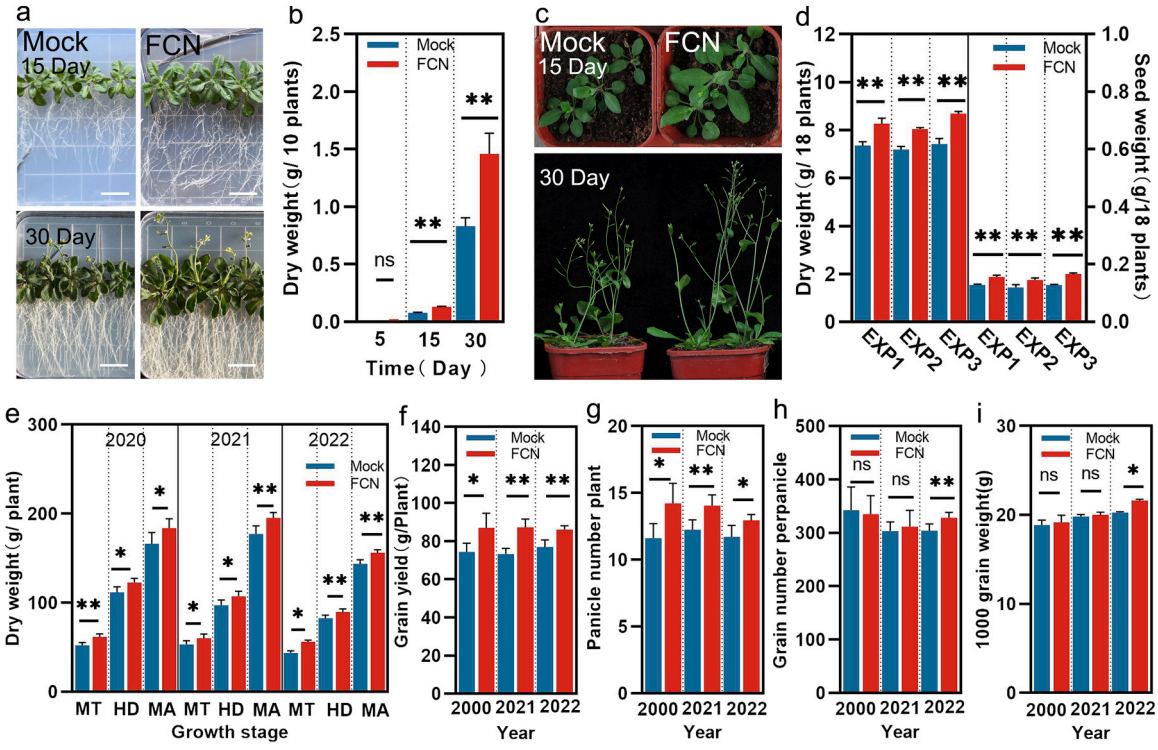

Fig. 6. FCN improves biomass and yields in *Arabidopsis* and rice. (a and b) Effects of FCN on the growth phenotype and biomass accumulation of *Arabidopsis* cultivated on MS medium. Scale bars, 1 cm. (c and d) Effects of FCN on the growth phenotype, biomass accumulation and seed yield of *Arabidopsis* cultivated in soil. Three independent experiments (EXP1, EXP2 and EXP3) were performed to investigate the growth regulation effects. (e-i) Effects of FCN on biomass accumulation, grain yield and rice yield components cultivated under natural conditions. MT, HD, and Ma in (e) indicate the growth stage of middle tillering, heading data and maturing, respectively. The error bars in the columns represent the SEM. The columns labeled with "* " and "* *" indicate significant differences at $P < 0.05$, and $P < 0.01$, respectively. "ns" means no significant difference.

FCN. Additionally, our results suggest that in the future, through ligand modification on the surface of nanoparticles, we can design and synthesize more efficient and targeted materials to induce more precise and specific resistance in plants. Same as gene editing technology, this new strategy could provide a stable and sustainable solution for crop production with reduced resource inputs.

Materials and methods

FCN Synthesis

FCN were prepared by an electrolysis method with some modifications. Two graphite plates (purity > 99.9%), as electrodes, were placed parallel with a separation of 20 cm in an electrolytic cell (3 L). Then, 2 L of distilled water was used as electrolyte and filled into the cell. Electrolysis was conducted at a DC voltage of approximately 3.0–5.0 V with a constant power of 0.5 watts. During the 15-day electrolysis period, the surface of the graphite plate was partially corroded, and the solution in the cell gradually changed from light brown to black (Fig. S1). The collosol was filtered using filter paper, and the resulting solution was further filtered through a 0.22 μm PVDF filter membrane with a vacuum suction filter to remove the residual graphite particles. Water-soluble FCN were obtained with a concentration of approximately 0.3%. The FCN collosol was freeze-dried to yield FCN powders. The reduced FCN (termed F500) were synthesized via thermal decomposition in a muffle furnace at 500 °C for 30 min.

Nanoparticles Characterization

The micro-morphology of FCN and F500 was examined using TEM (JEM-1011, Japan) and HRTEM (JEM-2010, Japan). The components and functional groups were analyzed on the FCN, F500, GO (purchased from Aladdin Co., Ltd.), and CNTs (purchased from Aladdin Co., Ltd.). FTIR spectra were recorded in dried KBr pellets (with a sample-to-KBr mass ratio of approximately 1:49) using a Bruker Tensor 37 spectrometer (Germany). The spectra were recorded at a range of 400–4000 cm^{-1} with 16 scans and a resolution of 4 cm^{-1}. XPS spectra were recorded at 40 eV pass energy using an Escalab 250Xi spectrometer (America) and a monochromatic Al Kα ($h\nu$ = 1486.6 eV) irradiation source at 75.0 W. The binding energy was calibrated with C1s= 284.8 eV.

Plant Materials, Growth Conditions, and Treatments. The model plant *Arabidopsis* (Col-0) and rice (cultivar Yongyou4949) were used as plant materials. Sterilized *Arabidopsis* seeds were treated with 2% (v/v) sodium hypochlorite for 1 min and placed on 1/2 Murashige and Skoog (MS) medium containing 3% sucrose and 0.8% agar and kept for 3 days at 4 °C in the dark to complete the vernalization. Subsequently, the plants were kept in a growth chamber for 20 days of culture under a day/night temperature of 24 °C/22 °C, PAR of 150 μmol m^{-2} s^{-1}, and a 16-hour photoperiod. The 20-day-old *Arabidopsis* seedlings were used for various measurements, and 20-day-old *Arabidopsis* seedlings were transplanted to MS medium containing 1.5 mg/L FCN or soil in pots for biomass and yield evaluation. For soil culture, one week after transplanting to the pots, the plants were watered twice with 50 mL per pot of 1/4 MS containing 1.5 mg/L FCN at an interval of 1 week and then watered with only 1/4 MS, as in the control. For high-temperature treatment, after twice FCN applications, the plants were transferred to a growth chamber with a constant temperature of 28 °C until maturation.

For the rice experiments, the seeds were germinated at 30 °C for 1 day, sown into a seedling tray, and cultured in a greenhouse. Then, the 30-day-old seedlings were transplanted with 10 hills per tank (length × width × depth of 120 cm × 60 cm × 60 cm) and cultivated outdoors in Beijing. One week after transplanting, each tank was treated with 30 L of water containing 1.5 mg/L FCN and 20 g of compound fertilizer. Throughout the growth period, a 1 cm water layer was maintained, and 15 g of urea was added to each tank just before heading.

Detection of ROS burst. ROS-sensitive probe H_2DCF-DA (Sigma-Aldrich) was used to visualize ROS burst in cells using LSM750 confocal laser-scanning microscope (Carl Zeiss AG, Germany). The first round of fully expanded leaves and root segments (1.5 cm) of the 20-day-old *Arabidopsis* or root segments (1.5 cm) of 7-day-old rice seedlings were dipped in sterile deionized water with 1 μg/mL H_2DCF-DA for 20 min at room temperature in the dark, cleaned with sterile water thrice to remove H_2DCF-DA attached, and incubated with 1.5 μg/mL of FCN, F500, GO, CNT and 3-FA (Aladdin). The time course (5, 15, 25, 35 and 45 min) of ROS-dependent green fluorescence (excitation at 488 nm and emission at 501–550 nm) was recorded, and the images were taken at the same settings and exposure time. The Image-J software was used to quantify the relative fluorescence intensity.

ROS burst was recorded using the luminol-based approach with TriStar2S LB 942 multimode reader (BERTHOLD Technologies, Germany). The first round of fully expanded leaves of 20-day-old *Arabidopsis*, which were about 5 mm in diameter, were collected and dipped in sterilized water in the dark for 4 h and replaced with deionized water every 30 min. Then, the leaves were transferred to 96-well plates and floated in 200 μL sterilized water for 30 min. Lastly, the water was replaced with a solution containing 30 μg/mL luminol (Sigma-Aldrich), 20 μg/mL HRP (Sigma-Aldrich) and 1.5 μg/mL FCN. Luminescence was detected for 60 min with a signal integration time of 60 s

Detection of ROS in chloroplasts. Protoplasts were used to visualize ROS in chloroplasts. *Arabidopsis* protoplast extraction was prepared using a plant protoplast preparation and transformation kit (Real-Times Biotechnology, Beijing, China) following the manufacturer's protocol. The protoplast was dipped in sterile deionized water with 1 μg/mL H_2DCF-DA for 5 min. Then, 1.5 μg/mL FCN was added, and the fluorescence signal was monitored within 0–40 min. The excitation wavelength was 488 nm. ROS-related fluorescence at 501–550 nm and chlorophyll autofluorescence at 640–735 nm were detected using an LSM750 confocal laser-scanning microscope. The Image J Colorization Finder plug-in was used to co-locate DCF and chloroplast spontaneous fluorescence.

Visualization of Ca2 + influx. The first round of fully expanded leaves of 20-day-old *Arabidopsis* was incubated in a growth chamber at 150 μmol m^{-2} s^{-1} light intensity in pretreatment buffer (50 mM KCl, 1 mM $CaCl_2$, 10 mM Tris-HCl, pH 7.5) for 2 h. Then, the leaves were washed several times with distilled water and suspended in 10 mM Tris-HCl buffer (pH 6.1) containing 18 μM Ca^{2+} fluorescent probe Fluo-3 AM in the dark for 20 min. Lastly, these samples were rinsed and incubated in 1.5 μg/mL FCN for 30 min, and green fluorescence was recorded using an LSM750 confocal laser-scanning microscope.

Visualization of FCN. The fluorescent probe fluorescein-5-isothiocyanate (FITC, Sigma-Aldrich) was labeled on FCN according to the reported method with minor modifications [65]. Then, 3 mg FITC was dissolved in 2 mL 50% (v/v) DMSO and was gradually added into 10 mL FCN with stirring at room temperature. The reaction solution was stirred continuously in the dark for 8 h and centrifuged using in 35 kDa ultrafiltration cube at 30,000 g for 15 min. The intercepted component, which was FCN tagged with FITC (FITC-FCN), was dissolved with an equal volume of water. FITC-FCN and FITC were added into *Arabidopsis* protoplasts, respectively. In addition, the first round of fully expanded leaves of 20-day-old *Arabidopsis* were soaked in FITC-FCN or FITC and vacuumed for 15 min. Then the leaves were rinsed by distilled water. FCN's location in the cell was recorded using an LSM750 confocal laser-scanning microscope. The Image J Colorization Finder plug-in was used to co-locate FITC-FCN and chloroplast spontaneous fluorescence.

Detection of H_2O_2. Here, 20-day-old *Arabidopsis* seedlings were transplanted into soil and cultured for 2 weeks. At noon, when the H_2O_2 reached their peak of the diurnal rhythm, they were sprayed with the same amount of deionized water or water containing 1.5 μg/mL of FCN. Then, the leaves were collected at the same position after 1/2/3/4 days after treatment. The content of H_2O_2 in the leaves was determined using the titanium sulfate method [66] with an EVOLUTION 220 spectrophotometer (Thermo, USA)·H_2O_2 was visualized by DAB staining, and images were taken using the Discovery V8 stereo microscope (Carl Zeiss AG, Germany). The intensity of DAB-staining was evaluated by Image J software.

Detection of enzyme-like activity of nanoparticles. SOD-like activities of nanoparticles were assessed based on the competition of nitroblue tetrazolium (NBT, Amresco) reduction. The inhibition rate of NBT oxidation to formazan was used to describe the SOD activities. Unless otherwise stated, the assays were conducted at room temperature with a 30 μg sample of nanoparticles (FCN, F500, GO, and CNT) or 25 ng of CuZnSOD (Sigma-Aldrich) in a 2 mL reaction.

Unless otherwise stated, the POD-like activities of nanoparticles were carried out at room temperature in a 1 mL reaction buffer (0.2 M NaAc, pH 3.5) containing 10 mM H_2O_2 and 1 mM TMB (Sigma) with 30 μg of nanoparticles or 20 ng of HRP (Sigma). Once the nanoparticles or HRP were added, a time scan of the OD at 653 nm was conducted by the EVOLUTION 220 spectrophotometer. The POD-like activities of FCN is much lower than HRP. To avoid the great difference in the data dimension, one unit of the POD-like activity was defined as an OD653 increase of 0.1 per minute in 1 mg of nanoparticles or 1 μg of protein for FCN and HRP, respectively. To investigate the kinetic characteristics of FCN, the assays were performed by changing the TMB concentrations at a fixed H_2O_2 concentration or vice versa.

To assess light-dependent oxidase-like activity, a 1 mL solution of 0.2 M NaAc (pH 3.5) containing 30 μg FCN and 5 mM ABTS was exposed to various light intensities (10, 50, 200, 500, 1000, 2000 μmol m^{-2} s^{-1}) for 20 min and then scanned at a wavelength range of 500–900 nm using an EVOLUTION 220 spectrophotometer. To evaluate the pH response of the oxidase-like activity of FCN and F500, the NaAc buffer was replaced with distilled water, and the pH was adjusted by adding HCl or NaOH, while the light intensity was kept at 1000 μmol m^{-2} s^{-1}. The ODs at 734 nm were recorded. The light-dependent oxidase-like activities of different nanoparticles were assessed at pH 4 and 7 in water containing 30 μg nanoparticles and 5 mM ABTS, and the light intensity was set at 1000 μmol m^{-2} s^{-1}.

RNA-Seq analysis. 20-day-old *Arabidopsis* seedlings were transferred to either MS medium (mock) or MS medium supplemented with 1.5 μg/mL FCN and then cultivated as described above. Then, the leaves were collected at 2 h, 6 h, 15 days, and 30 days after the treatment. For each treatment and time point, leaves from 3 different plants were collected together as a replicate, and five biological replicates were collected. Samples were frozen and ground in liquid nitrogen. Total mRNA was extracted using Trizol reagent (Invitrogen) and shipped to BerryGenomics for library construction and sequencing. Briefly, RNA was purified using an RNeasy MinElute Cleanup kit (QIAGEN) and the quality was examined on the NanoDrop 2000 (Thermo Scientific) and Bioanalyzer 2100 system (Agilent Technologies). RNA library was constructed using the NEBNext Ultra RNA Library Prep Kit for Illumina (NEB) with 1 mg RNA per sample. Then, the constructed library was inspected with Qubit 2.0 Fluorometer (Life Technologies) and Bioanalyzer 2100 system. Sequencing was performed on the Illumina Hiseq platform (2 ×150-bp read length). Then the raw reads were cleaned up and aligned to the *Arabidopsis* reference genome (TAIR10). Gene-expression levels were calculated using the fragments per kb of transcript per million fragments mapped reads (FPKM) method. Differential expression genes with FDR< 0.05 and |log2(fold change)|> 1 were screened using the DESeq2 software. Gene Ontology (GO) enrichment online analyses were conducted using PANTHER (http://pantherdb.org/), and GO terms with FDR< 0.05 were screened.

For RT–qPCR gene expression analysis, one microgram of RNA was used for reverse transcription using the RevertAid First Strand cDNA Synthesis Kit (Thermo Scientific). Real-time qPCR analysis was performed using the Talent qPCR PreMix (SYBRGreen) Kit (Tiangen) on an ABI Quant Studio6 real-time machine (Bio-Rad). The *Arabidopsis* EF gene was used as the reference gene for normalization. Primer sequences for quantitative PCR are listed in Supplementary Table 2.

CRediT authorship contribution statement

Zhijiang Guo: Conceptualization, Investigation, Writing – original draft. **Qiong Chen**: Conceptualization, Investigation, Writing – review & editing. **Taibo Liang:** Investigation, Writing – review & editing. **Baoyuan Zhou**: Investigation, Writing – review & editing. **Suhua Huang**: Investigation, Writing – review & editing. **Xiufeng Cao**: Writing – review & editing. **Xiuli Wang**: Conceptualization, Methodology, Supervision. **Zaisong Ding**: Conceptualization, Methodology, Supervision, Project administration, Writing – original draft, Writing – review & editing. **Jiangping Tu**: Conceptualization, Methodology, Supervision, Project administration, Writing – review & editing.

Declaration of Competing Interest

The authors declare that they have no known competing financial interests or personal relationships that could have appeared to influence the work reported in this paper.

Data Availability

Data will be made available on request.

Acknowledgment

This work was supported by CAAS Science and Technology Innovation Program (2060302-2), the National Natural Science Foundation of China (32071957), the Postdoctoral Research Startup Fund of the University of Jinan (No. 1003887) and the National Natural Science Foundation of China (Grant No. 42007112). The authors appreciate Professor Rongxiang Fang from the Institute of Microbiology, CAS, Professor Jianping Xie from ZhengzhouTobacco Research Institute of CNTC, Professor Xiaochun Qin from Jinan University, and Professor Changdong Gu from Zhejiang University for kindly providing suggestions on the manuscript.

Appendix A. Supporting information

Supplementary data associated with this article can be found in the online version at doi:10.1016/j.nantod.2023.102045.

References

[1] Z. He, S. Webster, S.Y. He, Growth-defense trade-offs in plants, Curr. Biol.. 32 (2022) 634–639.
[2] H. Zhang, Y. Zhao, J.-K. Zhu, Thriving under stress: how plants balance growth and the stress response, Dev. Cell. 55 (5) (2020) 529–543.
[3] B. Huot, J. Yao, B.L. Montgomery, S.-Y. He, Growth-defense tradeoffs in plants: a balancing act to optimize fitness, Mol. Plant. 7 (2014) 1267–1287.
[4] R. Mittler, S.I. Zandalinas, Y. Fichman, Van, F. Breusegem, Reactive oxygen species signalling in plant stress responses, Nat. Rev. Mol. Cell Biol.. 23 (2022) 663–679.
[5] P. Köster, T.A. DeFalco, C. Zipfel, Ca^{2+} signals in plant immunity, EMBO J. 41 (2022), e110741.
[6] R. Waadt, C.A. Seller, P.-K. Hsu, Y. Takahashi, S. Munemasa, J.I. Schroeder, Plant hormone regulation of abiotic stress responses, Nat. Rev. Mol. Cell Biol.. 23 (2022) 680–694.
[7] M. Hussain, N. Shakoor, M. Adeel, M.A. Ahmad, H. Zhou, Z. Zhang, M. Xu, Y. Rui, J.C. White, Nano-enabled plant microbiome engineering for disease resistance, Nano Today 48 (2023), 101752.

[8] R. Mittler, E. Blumwald, The roles of ROS and ABA in systemic acquired acclimation, Plant Cell 27 (2015) 64–70.
[9] J. Lozano-Juste, L. Infantes, I. Garcia-Maquilon, R. Ruiz-Partida, E. Merilo, J. L. Benavente, A. Velazquez-Campoy, A. Coego, M. Bono, J. Forment, B. Pampín, P. Destito, A. Monteiro, R. Rodríguez, J. Cruces, P.L. Rodriguez, A. Albert, Structure-guided engineering of a receptor-agonist pair for inducible activation of the ABA adaptive response to drought, Sci. Adv.. 9 (10) (2023), eade9948.
[10] J. Kourelis, C. Marchal, S. Kamoun, NLR immune receptor-nanobody fusions confer plant disease resistance, Science 379 (2023) 937–939.
[11] H. Kollist, S.I. Zandalinas, S. Sengupta, M. Nuhkat, J. Kangasjärvi, R. Mittler, Rapid responses to abiotic stress: priming the landscape for the signal transduction network, Trends Plant Sci. 24 (2019) 25–37.
[12] Y. Fichman, R. Mittler, Integration of electric, calcium, reactive oxygen species and hydraulic signals during rapid systemic signaling in plants, Plant J. 107 (2021) 7–20.
[13] Y. Fichman, R. Mittler, Rapid systemic signaling during abiotic and biotic stresses: is the ROS wave master of all trades? Plant J. 102 (2020) 887–896.
[14] Y. Kadota, K. Shirasu, C. Zipfel, Regulation of the NADPH oxidase RBOHD during plant immunity, Plant Cell Physiol. 56 (2015) 1472–1480.
[15] Y. Fichman, G. Miller, R. Mittler, Whole-plant live imaging of reactive oxygen species, Mol. Plant. 12 (2019) 1203–1210.
[16] H. Sies, D.P. Jones, Reactive oxygen species (ROS) as pleiotropic physiological signaling agents, Nat. Rev. Mol.. Cell Biol.. 21 (2020) 363–383.
[17] R. Mittler, ROS are good, Trends Plant Sci. 22 (2017) 11–19.
[18] R.P. Mendoza, J.M. Brown, Engineered nanomaterials and oxidative stress: current understanding and future challenges, Curr. Opin. Toxicol. 13 (2019) 74–80.
[19] M. Sanati, A.R. Afshari, P. Kesharwani, V.N. Sukhorukov, A. Sahebkar, Recent trends in the application of nanoparticles in cancer therapy: the involvement of oxidative stress, J. Control. Release 348 (2022) 287–304.
[20] S. Kwon, H. Ko, D.G. You, K. Kataoka, J.H. Park, Nanomedicines for reactive oxygen species mediated approach: an emerging paradigm for cancer treatment, Acc. Chem. Res. 52 (2019) 1771–1782.
[21] Y. Wang, R. Cai, C. Chen, The nano-bio interactions of nanomedicines: understanding the biochemical driving forces and redox reactions, Acc. Chem. Res. 52 (2019) 1507–1518.
[22] G.V. Lowry, A. Avellan, L.M. Gilbertson, Opportunities and challenges for nanotechnology in the agri-tech revolution, Nat. Nanotechnol. 14 (2019) 517–522.
[23] M. Chandel, K. Kaur, B.K. Sahu, S. Sharma, R. Panneerselvam, V. Shanmugam, Promise of nano-carbon to the next generation sustainable agriculture, Carbon 188 (2022) 461–481.
[24] S.K. Verma, A.K. Das, S. Gantait, V.3 Kumar, E. Gurel, Applications of carbon nanomaterials in the plant system: a perspective view on the pros and cons, Sci. Total Environ. 667 (2019) 485–499.
[25] G. Zhai, S.M. Gutowski, K.S. Walters, B. Yan, J.L. Schnoor, Charge, size, and cellular selectivity for multiwall carbon nanotubes by maize and soybean, Environ. Sci. Technol. 49 (2015) 7380–7390.
[26] Y. Li, Z. Tang, Z. Pan, R. Wang, X. Wang, P. Zhao, M. Liu, Y. Zhu, C. Liu, W. Wang, Q. Liang, J. Gao, Y. Yu, Z. Li, B. Lei, J. Sun, Calcium-mobilizing properties of salvia miltiorrhiza-derived carbon dots confer enhanced environmental adaptability in plants, ACS Nano 16 (2022) 4357–4370.
[27] T.A. Swift, D. Fagan, D. Benito-Alifonso, S.A. Hill, M.L. Yallop, T.A.A. Oliver, T. Lawson, M.C. Galan, H.M. Whitney, Photosynthesis and crop productivity are enhanced by glucose-functionalised carbon dots, New Phytol. 229 (2021) 783–790.
[28] H. Ming, Z. Ma, Y. Liu, K. Pan, H. Yu, F. Wang, Z. Kang, Large scale electrochemical synthesis of high quality carbon nanodots and their photocatalytic property, Dalton Trans. 41 (2012) 9526–9531.
[29] H. Yang, Y. Liu, Z. Guo, B. Lei, J. Zhuang, X. Zhang, Z. Liu, C. Hu, Hydrophobic carbon dots with blue dispersed emission and red aggregation-induced emission, Nat. Commun. 10 (2019) 1789.
[30] D.B. Pal, A. Singh, J.M. Jha, N. Srivastava, A. Hashem, M.A. Alakeel, E.F. Abd Allah, V.K. Gupta, Low-cost biochar adsorbents prepared from date and delonix regia seeds for heavy metal sorption, Bioresour. Technol. 339 (2021), 125606.
[31] F. Ma, J. Nian, C. Bi, M. Yang, C. Zhang, L. Liu, H. Dong, M. Zhu, B. Dong, Preparation of carboxylated graphene oxide for enhanced adsorption of U(VI), J. Solid State Chem. 277 (2019) 9–16.
[32] A. Kivinen, M. Ovaska, Polarized infrared spectra of hydrogen-bonded systems by the stretched-polymer method. dimers of carboxylic acids, J. Phys. Chem. 87 (20) (1983) 3809–3811.
[33] D. Xu, L. Wu, H. Yao, L. Zhao, Catalase-like nanozymes: classification, catalytic mechanisms, and their applications, Small 8 (2022), e2203400.
[34] C. Dong, S. Wang, M. Ma, P. Wei, Y. Chen, A. Wu, Z. Zha, H. Bi, Inhibition of oxidative stress in vivo through enzyme-like activity of carbon dots, Appl. Mater. Today 25 (2021), 101178.
[35] H. Sun, A. Zhao, N. Gao, K. Li, J. Ren, X. Qu, Deciphering a nanocarbon-based artificial peroxidase: chemical identification of the catalytically active and substrate-binding sites on graphene quantum dots, Angew. Chem. Int. Ed. 54 (2015) 7176–7180.
[36] H. Wei, E. Wang, Fe_3O_4 magnetic nanoparticles as peroxidase mimetics and their applications in H_2O_2 and glucose detection, Anal. Chem. 80 (2008) 2250–2254.
[37] M. Yuan, Z. Jiang, G. Bi, K. Nomura, M. Liu, Y. Wang, B. Cai, J.-M. Zhou, S.Y. He, X.-F. Xin, Pattern-recognition receptors are required for NLR-mediated plant immunity, Nature 592 (2021) 105–109.
[38] C. Zipfel, G. Kunze, D. Chinchilla, A. Caniard, J.D.G. Jones, T. Boller, G. Felix, Perception of the bacterial PAMP EF-Tu by the receptor EFR restricts agrobacterium-mediated transformation, Cell 125 (2006) 749–760.
[39] S. Ranf, N. Gisch, M. Schäffer, T. Illig, L. Westphal, Y.A. Knirel, P.M. Sánchez-Carballo, U. Zähringer, R. Hückelhoven, J. Lee, D. Scheel, A lectin S-domain receptor kinase mediates lipopolysaccharide sensing in arabidopsis thaliana, Nat. Immunol. 16 (2015) 426–433.
[40] B.-Q. Gong, F.-Z. Wang, J.-F. Li, Hide-and-seek: chitin-triggered plant immunity and fungal counterstrategies, Trends Plant Sci. 25 (2020) 805–816.
[41] A. Kutschera, C. Dawid, N. Gisch, C. Schmid, L. Raasch, T. Gerster, M. Schäffer, E. Smakowska-Luzan, Y. Belkhadir, A.C. Vlot, C.E. Chandler, R. Schellenberger, D. Schwudke, R.K. Ernst, S. Dorey, R. Hückelhoven, T. Hofmann, S. Ranf, Bacterial medium-chain 3-hydroxy fatty acid metabolites trigger immunity in arabidopsis plants, Science 364 (2019) 178–181.
[42] M. Bjornson, P. Pimprikar, T. Nürnberger, C. Zipfel, The transcriptional landscape of arabidopsis thaliana pattern-triggered immunity, Nat. Plants 7 (5) (2021) 579–586.
[43] Y. Peng, R. van Wersch, Y. Zhang, Convergent and divergent signaling in PAMP-triggered immunity and effector triggered immunity, Mol. Plant Microbe Interact. 31 (2018) 403–409.
[44] P. Li, L. Zhao, F. Qi, N.M.P.S. Htwe, Q. Li, D. Zhang, F. Lin, K. Shang-Guan, Y. Liang, The receptor-like cytoplasmic kinase RIPK regulates broad-spectrum ROS signaling in multiple layers of plant immune system, Mol. Plant. 14 (2021) 1652–1667.
[45] S.I. Zandalinas, Y. Fichman, A.R. Devireddy, S. Sengupta, R.K. Azad, R. Mittler, Systemic signaling during abiotic stress combination in plants, PNAS 117 (2020) 13810–13820.
[46] B.P.M. Ngou, P. Ding, J.D.G. Jones, Thirty years of resistance: zig-zag through the plant immune system, Plant Cell 34 (2022) 1447–1478.
[47] S. Lolle, D. Stevens, G. Coaker, Plant NLR-triggered Immunity: from receptor activation to downstream signaling, Curr. Opin. Immunol. 62 (2020) 99–105.
[48] S. Tian, X. Wang, P. Li, H. Wang, H. Ji, J. Xie, Q. Qiu, D. Shen, H. Dong, Plant aquaporin AtPIP14 links apoplastic H_2O_2 induction to disease immunity pathways, Plant Physiol. 171 (2016) 1635–1650.
[49] M. Toyota, D. Spencer, S. Sawai-Toyota, W. Jiaqi, T. Zhang, A.J. Koo, G.A. Howe, S. Gilroy, Glutamate triggers long-distance, calcium-based plant defense signaling, Science 361 (2018) 1112–1115.
[50] C. Sözen, S.T. Schenk, M. Boudsocq, C. Chardin, M. Almeida-Trapp, A. Krapp, H. Hirt, A. Mithöfer, J. Colcombet, Wounding and insect feeding trigger two independent MAPK pathways with distinct regulation and kinetics, Plant Cell 32 (2020) 1988–2003.
[51] M. Li, C. Kim, Chloroplast ROS and stress signaling, Plant Commun. 3 (2022), 100264.
[52] B. Castro, M. Citterico, S. Kimura, D.M. Stevens, M. Wrzaczek, G. Coaker, Stress-induced reactive oxygen species compartmentalization, perception and signalling, Nat. Plants 7 (2021) 403–412.
[53] H.-J. Lee, P.J. Seo, Ca^{2+}talyzing initial responses to environmental stresses, Trends Plant Sci. 26 (8) (2021) 849–870.
[54] Y. Fichman, R. Mittler, Integration of electric, calcium, reactive oxygen species and hydraulic signals during rapid systemic signaling in plants, Plant J. 107 (1) (2021) 7–20, https://doi.org/10.1111/tpj.15360.
[55] G.-H. Lim, M.B. Shine, L. de Lorenzo, K. Yu, W. Cui, D. Navarre, A.G. Hunt, J.-Y. Lee, A. Kachroo, P. Kachroo, Plasmodesmata localizing proteins regulate transport and signaling during systemic acquired immunity in plants, Cell Host Microbe 19 (4) (2016) 541–549.
[56] Y. Fichman, R.J. Myers, D.G. Grant, R. Mittler, Plasmodesmata-localized proteins and ROS orchestrate light-induced rapid systemic signaling in arabidopsis, Sci. Signal 14 (2021), eabf0322.
[57] V. Dogra, R.M. Singh, M. Li, M. Li, S. Singh, C. Kim, EXECUTER2 modulates the EXECUTER1 signalosome through its singlet oxygen-dependent oxidation, Mol. Plant. 15 (3) (2022) 438–453.
[58] S.I. Zandalinas, S. Sengupta, D. Burks, R.K. Azad, R. Mittler, Identification and characterization of a core set of ROS wave-associated transcripts involved in the systemic acquired acclimation response of arabidopsis to excess light, Plant J. 98 (2019) 126–141.
[59] M. Hrmova, S.S. Hussain, Plant transcription factors involved in drought and associated stresses, Int. J. Mol. Sci. 22 (2021) 5662.
[60] K. Feng, X.-L. Hou, G.-M. Xing, J.-X. Liu, A.-Q. Duan, Z.-S. Xu, M.-Y. Li, J. Zhuang, A.-S. Xiong, Advances in AP2/ERF super-family transcription factors in plant, Crit. Rev. Biotechnol. 40 (2020) 750–776.
[61] J. Jiang, S. Ma, N. Ye, M. Jiang, J. Cao, J. Zhang, WRKY transcription factors in plant responses to stresses, J. Integr. Plant Biol. 59 (2017) 86–101.
[62] H. Tsukagoshi, W. Busch, P.N. Benfey, Transcriptional regulation of ROS controls transition from proliferation to differentiation in the root, Cell 143 (2010) 606–616.
[63] B. Orman-Ligeza, B. Parizot, R. de Rycke, A. Fernandez, E. Himschoot, F. Van Breusegem, M.J. Bennett, C. Périlleux, T. Beeckman, X. Draye, RBOH-mediated ROS production facilitates lateral root emergence in arabidopsis, Development 143 (2016) 3328–3339.
[64] X. Yan, S. Chen, Z.-Y. Pan, W.-C. Zhao, Y.-K. Rui, L.-J. Zhao, AgNPs-triggered seed metabolic and transcriptional reprogramming enhanced rice salt tolerance and blast resistance, ACS Nano 17 (2023) 492–504.
[65] M. Tang, P. Teng, Y. Long, X. Wang, L. Liang, D. Shen, J. Wang, H. Zheng, Hollow carbon dots labeled with FITC or TRITC for use in fluorescent cellular imaging, Mikrochim. Acta 14 (2018) 223.
[66] C.N. Satterfield, A.H. Bonnell, Interferences in titanium sulfate method for hydrogen peroxide, Anal. Chem. 27 (7) (1955) 1174–1175.